ACS Partner Journal
PRECISION CHEMISTRY

pubs.acs.org/PrecisionChem
Article

High-Performance H_2 Photosynthesis from Pure Water over Ru−S Charge Transfer Channels

Published as part of Precision Chemistry virtual special issue "Precision Chemistry for the Hydrogen Cycle".

Huiping Peng, Mingzi Sun, Fei Xue, Xiaozhi Liu, Shangheng Liu, Tang Yang, Lin Sun, Hongbo Geng, Dong Su, Bolong Huang,* Yong Xu,* and Xiaoqing Huang*

Cite This: *Precis. Chem.* 2024, 2, 471−479
Read Online

ACCESS | Metrics & More | Article Recommendations | Supporting Information

ABSTRACT: As a versatile energy carrier, H_2 is considered as one of the most promising sources of clean energy to tackle the current energy crisis and environmental concerns, which can be produced from photocatalytic water splitting. However, solar-driven photocatalytic H_2 production from pure water in the absence of sacrificial reagents remains a great challenge. Herein, we demonstrate that the incorporation of Ru single atoms (SAs) into $ZnIn_2S_4$ (Ru-ZIS) can enhance the light absorption, reduce the energy barriers for water dissociation, and construct a channel (Ru−S) for separating photogenerated electron−hole pairs, as a result of a significantly enhanced photocatalytic water splitting process. Impressively, the productivity of H_2 reaches 735.2 μmol g^{-1} h^{-1} under visible light irradiation in the absence of sacrificial agents. The apparent quantum efficiency (AQE) for H_2 evolution reaches 7.5% at 420 nm, with a solar-to-hydrogen (STH) efficiency of 0.58%, which is much higher than the value of natural synthetic plants (∼0.10%). Moreover, Ru-ZIS exhibits steady productivity of H_2 even after exposure to ambient conditions for 330 days. This work provides a unique strategy for constructing charge transfer channels to promote the separation of photogenerated electron−hole pairs, which may motivate the fundamental researches on catalyst design for photocatalysis and beyond.

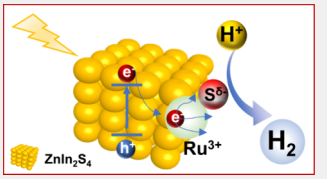

KEYWORDS: *Ru single atom, charge channel, $ZnIn_2S_4$, photocatalytic, pure water splitting*

1. INTRODUCTION

As a versatile energy carrier, H_2 has attracted great interest because of its renewability, clean combustion product, and high energy density.[1−3] Recently, solar-driven water splitting has been regarded as a fascinating strategy for harvesting solar energy to produce clean and renewable H_2.[4,5] Numerous photocatalysts, including TiO_2,[6] ZnO,[7] WO_3,[8] CdS,[9] and $BiVO_4$,[10] have been employed for triggering water splitting to generate H_2 under light irradiation. However, the high-efficiency photocatalytic water splitting, especially in the absence of sacrificial agents, is largely blocked by drawbacks, including limited sunlight wavelength response and rapid recombination of photogenerated electron−hole pairs. To promote the H_2 productivity from solar-driven water splitting, a common strategy is introducing sacrificial reagent to consume the photogenerated holes for suppressing the recombination of electron−hole pairs.[11,12] Nevertheless, such strategy will inevitably bring new environmental concerns, increase the cost of H_2 production, and undermine the research advances.[13,14]

A typical ternary sulfide, two-dimensional (2D) hexagonal $ZnIn_2S_4$ (ZIS), has attracted increasing attention because of its unique physicochemical properties.[15,16] Nevertheless, the extensive application of ZIS in photocatalysis with visible light is limited by its low concentration of photogenerated carriers and fast recombination of photogenerated electron−hole pairs.[17,18] To realize the photocatalytic H_2 evolution over ZIS, one needs to modify ZIS to increase the absorption of visible light and especially to suppress the recombination of photogenerated electron−hole pairs without any sacrificial agents. Recently, the introduction of heteroatoms has been regarded as one of the most popular strategies for modifying the band structure of semiconductors and facilitate the migration of photogenerated carriers.[19−21] Nevertheless, this structure engineering may bring undesired defects, thereby providing sites for the recombination of photogenerated electron−hole pairs.[22,23] Consequently, constructing a channel for the oriented migration of electrons and holes is vital for photocatalysis yet is extremely challenging.

In this work, we have demonstrated that Ru single atoms (SAs) anchored on $ZnIn_2S_4$ (Ru-ZIS) via Ru−S bonds can serve as a highly efficient photocatalyst for pure water splitting to produce H_2 under visible light irradiation without any sacrificial reagent. *In situ* X-ray photoelectron spectroscopy, *in situ* electron paramagnetic resonance, and *in situ* X-ray

Received: April 8, 2024
Revised: May 15, 2024
Accepted: June 4, 2024
Published: June 12, 2024

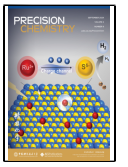

https://doi.org/10.1021/prechem.4c00035
Precis. Chem. 2024, 2, 471−479

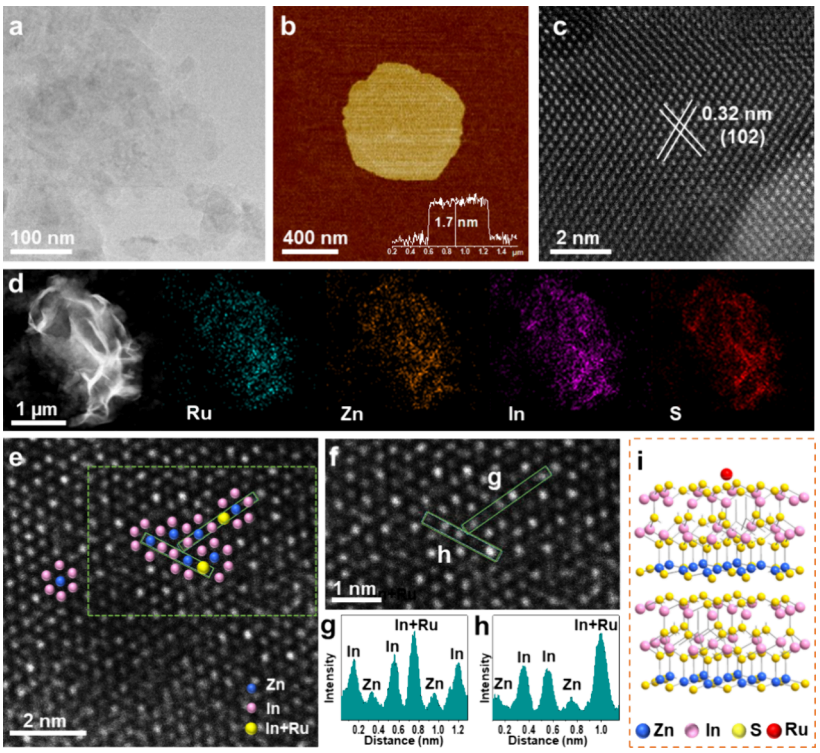

Figure 1. Characterization of the physical structure of Ru-ZIS. (a) TEM image, (b) AFM image, (c) HRTEM image, and (d) HAADF-STEM image with elemental mappings of Ru-ZIS. (e) HAADF-STEM image of Ru-ZIS, (f) Magnified HAADF-STEM image of Ru-ZIS. (g,h) Strength profiles from the areas labeled by green rectangle. (i) Scheme of Ru-ZIS.

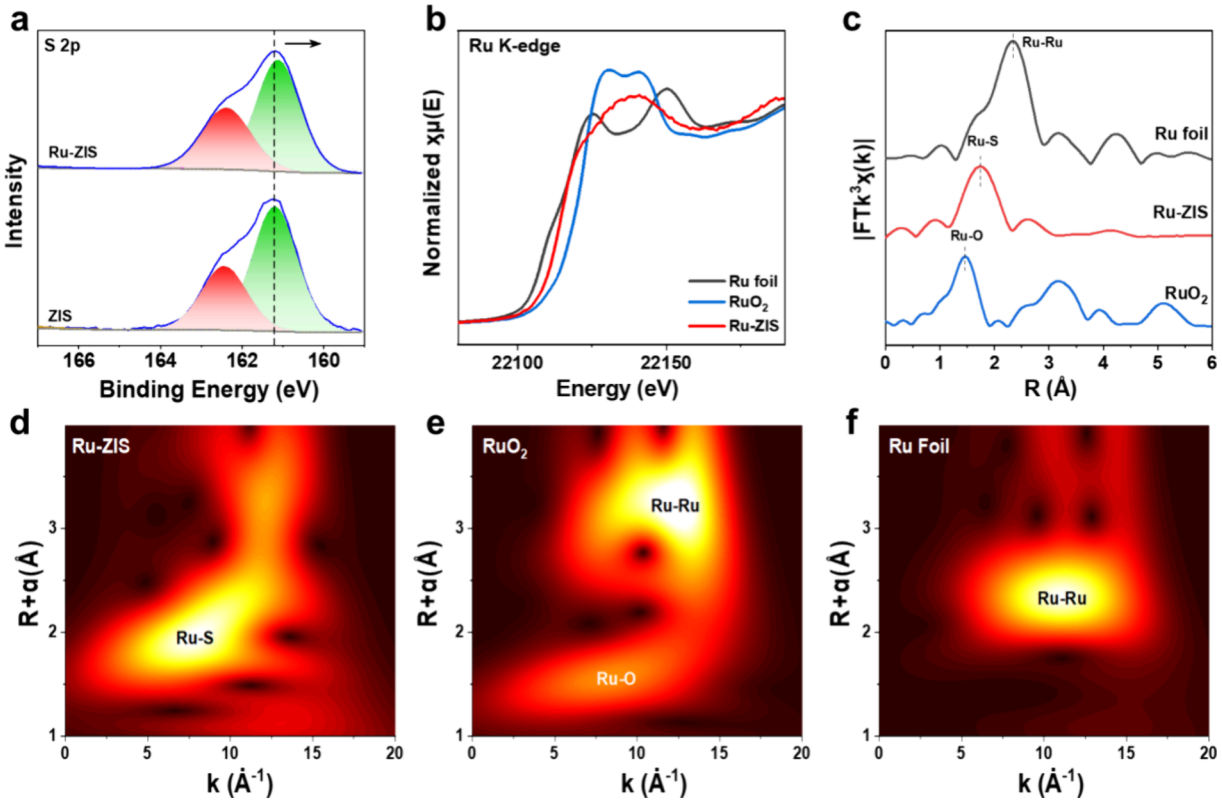

Figure 2. EXAFS characterization. (a) S 2p XPS spectra of Ru-ZIS and ZIS. (b) Ru K-edge XANES spectra of Ru-ZIS, RuO_2, and Ru foil. (c) Fourier transforms of k^3-weighted Ru K-edge of EXAFS spectra of Ru-ZIS, RuO_2, and Ru foil. (d−f) Wavelet transform (WT)-EXAFS of the Ru-ZIS, RuO_2, and Ru foil.

https://doi.org/10.1021/prechem.4c00035
Precis. Chem. 2024, 2, 471−479

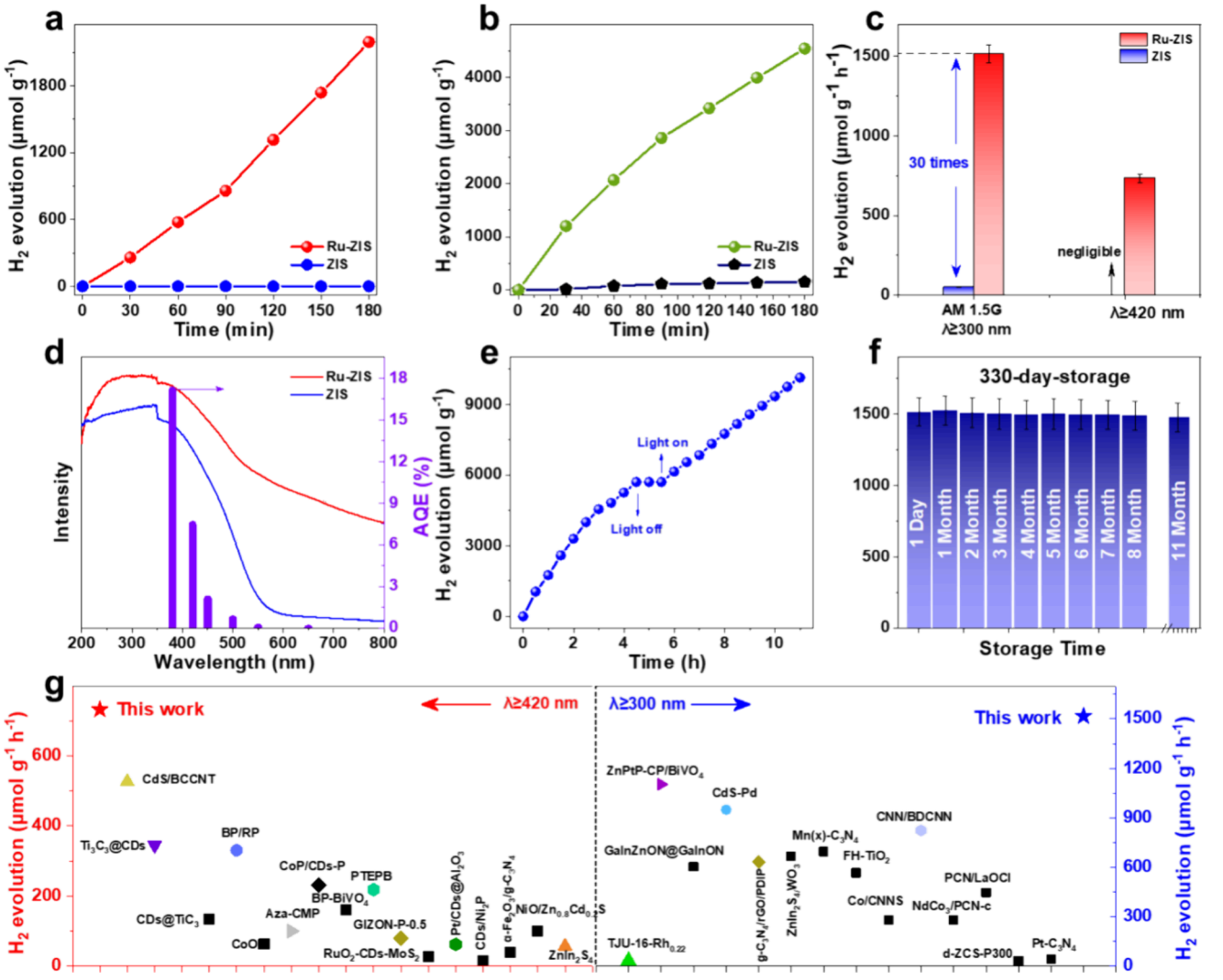

Figure 3. Photocatalytic performance. (a) Photocatalytic H_2 evolution rates of various catalysts under the irradiation of visible light ($\lambda \geq 420$ nm) and (b) simulated solar light (AM 1.5G, $\lambda \geq 300$ nm). (c) H_2 productivity of Ru-ZIS under the irradiation of simulated solar light (AM 1.5G, $\lambda \geq 300$ nm) and visible light irradiation ($\lambda \geq 420$ nm) for 3 h. (d) AQE of Ru-ZIS under different wavelengths. (e) H_2 evolution over Ru-ZIS with and without the irradiation with simulated light (AM 1.5G, $\lambda \geq 300$ nm). (f) Catalytic performance of Ru-ZIS after exposure to ambient environment for 330 days. Light source: AM 1.5G, $\lambda \geq 300$ nm. (g) Comparison between Ru-ZIS and other reported photocatalysts for pure water splitting.

absorption spectroscopy, as well as density functional theory (DFT) calculations, reveal that the incorporation of Ru SAs into ZIS can provide a channel for the photogenerated electron transfer from Ru to S via Ru−S coordination as a result of enhanced separation of electron−hole pairs. Ru-ZIS displays a H_2 productivity of 735.2 μmol g^{-1} h^{-1} under visible light irradiation in the absence of sacrificial agents. Moreover, Ru-ZIS exhibits steady productivity of H_2 even after exposure to ambient conditions for 330 days. Impressively, the apparent quantum efficiency (AQE) for H_2 evolution over Ru-ZIS reaches 7.5% at 420 nm, and the solar-to-hydrogen (STH) efficiency reaches 0.58%, which is much higher than that of a natural synthetic plant (~0.10%).

2. RESULTS AND DISCUSSION

Ru-ZIS was fabricated via a wet-chemical approach using $RuBr_3$, $Zn(CH_3COO)_2{\cdot}2H_2O$, $InCl_3$, and thioacetamide (TAA) as precursors (see the Experimental Section in the Supporting Information for details). The content of Ru in Ru-ZIS was determined to be 1.3 wt % by inductively coupled plasma optical emission spectroscopy (ICP-OES) analysis (Table S1). The products are present as 2D nanosheets (Figure 1a and Figure S1) with a mean thickness of ~1.7 nm on the basis of atomic force microscopy (AFM, Figure 1b). The lattice distance of 0.32 nm in the high-resolution transmission electron microscopy (HRTEM) image can be indexed as the (102) facet of hexagonal $ZnIn_2S_4$ (Figure 1c). Elemental mappings show that Zn, In, S, and Ru are uniformly distributed in the Ru-ZIS (Figure 1d). Moreover, the X-ray diffraction (XRD) pattern of Ru-ZIS exhibits features similar to those of pure ZIS (JCPDS No. 65-2023), suggesting that the main structure of ZIS was largely maintained after introducing Ru SAs (Figure S2). Besides, the absence of Ru peaks in the XRD pattern of Ru-ZIS can be attributed to the high dispersity of Ru atoms, which has been further validated by the similar features in the Fourier transform infrared (FTIR) and Raman spectra of ZIS and Ru-ZIS (Figure S3). Furthermore, aberration-corrected high-angle annular dark field scanning transmission electron microscopy (AC-HAADF-STEM) images of ZIS and Ru-ZIS were collected to investigate the

https://doi.org/10.1021/prechem.4c00035
Precis. Chem. 2024, 2, 471−479

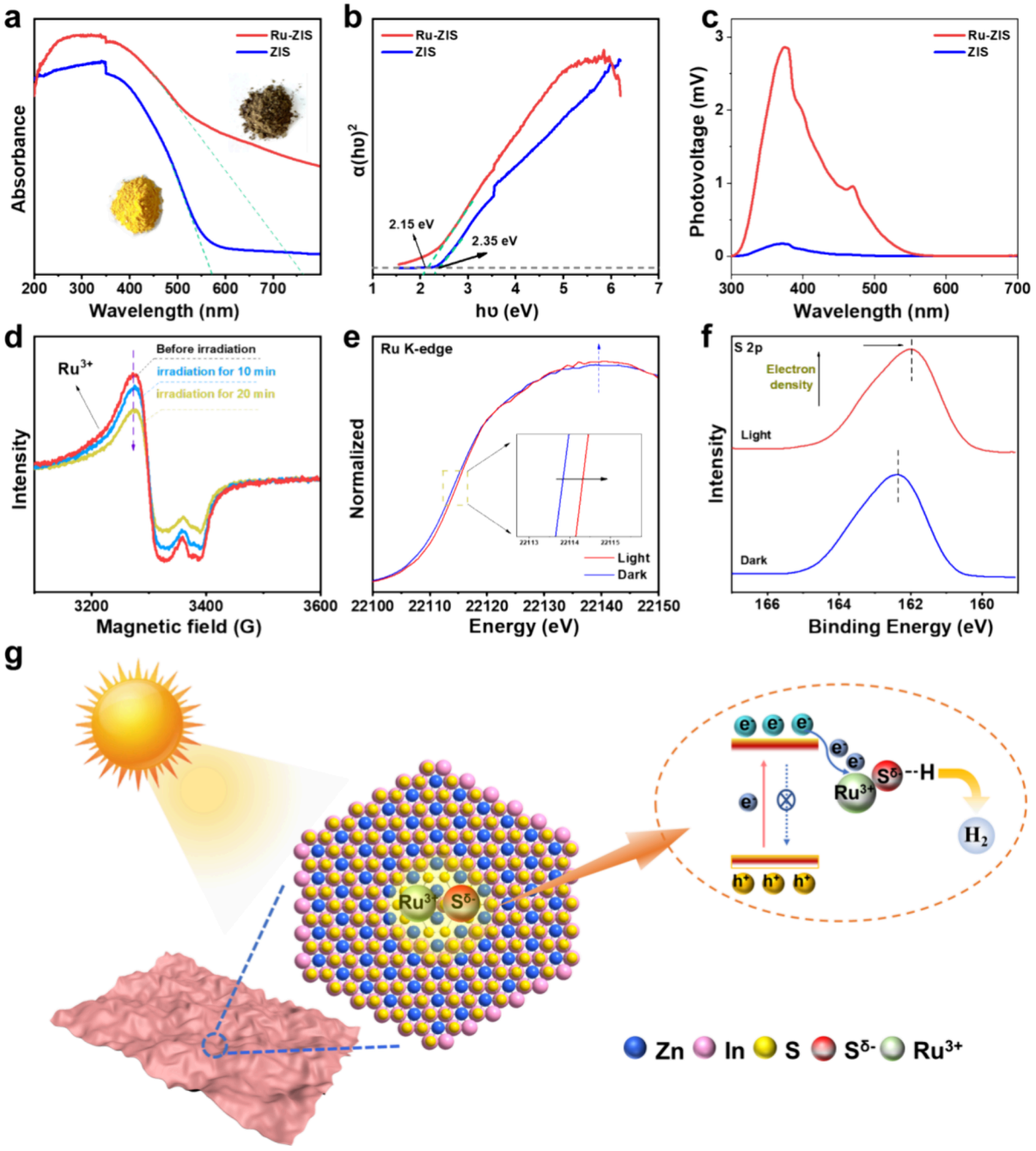

Figure 4. Energy transfer investigation. (a) UV−vis absorption spectra and (b) $(\alpha h\nu)^2$ versus $h\nu$ curves of Ru-ZIS and ZIS. (c) Stable-state SPV spectra of Ru-ZIS and ZIS. (d) Solid-state *in situ* EPR spectra of Ru-ZIS under visible light irradiation ($\lambda \geq 420$ nm). (e) *In operando* XANES spectra of Ru-ZIS at the Ru K-edge. (f) XPS spectra of S 2p for Ru-ZIS in the dark and under visible light irradiation. (g) Schematic diagram of photocatalytic H_2 evolution on Ru-ZIS via pure water splitting under visible light irradiation.

structures of the introduced Ru atoms. Considering the different atomic numbers of Zn, In, and Ru (In > Ru > Zn), Ru atoms can be likely identified by the different brightness in the AC-HAADF-STEM image of Ru-ZIS (Figure 1e−h).[24] Compared with the AC-HAADF-STEM image of pure ZIS (Figure S4), Ru atoms have been successfully incorporated onto ZIS as single state (Figure 1g,h), as vividly depicted by the schematic model of in Figure 1i.[25]

Subsequently, X-ray photoelectron spectroscopy (XPS) was conducted to investigate the electronic properties of Ru-ZIS. Compared with ZIS, no obvious changes were observed in the Zn 2p and In 3d XPS spectra of Ru-ZIS (Figure S5). For the S 2p XPS spectrum of Ru-ZIS, the peak negatively shifts by ∼0.2 eV compared with that of ZIS, thereby indicating the strong interaction between Ru and S (Figure 2a).[26] In the electron paramagnetic resonance (EPR) spectra of ZIS and Ru-ZIS, the similar peak intensity corresponding to S vacancies (S_v) implies that Ru introduction hardly contributes to the formation of S_v (Figure S6). Note that the intense peak in the EPR spectrum of Ru-ZIS corresponds to Ru^{3+} (Figure S6).[27,28] Furthermore, X-ray absorption near edge structure (XANES) and extended X-ray absorption fine structure (EXAFS) spectra were collected to investigate the coordination structure and electronic properties of Ru in Ru-ZIS. In comparison with

https://doi.org/10.1021/prechem.4c00035
Precis. Chem. 2024, 2, 471−479

the XANES spectrum of Ru-ZIS at Ru K-edge with those of Ru foil and RuO_2, Ru in Ru-ZIS mainly presents as oxidation state ($Ru^{\delta+}$, $0 < \delta < 4$) (Figure 2b), which is in line with EPR result. In the EXAFS spectrum of Ru-ZIS, different from the peaks of Ru−O (1.7 Å) and Ru−Ru coordination (2.4 Å) in the EXAFS spectra of RuO_2 and Ru foil, respectively, the sharp peak at ∼1.9 Å is ascribed to Ru−S coordination (Figure 2c).[29] The absence of Ru−Ru coordination in the EXAFS spectrum of Ru-ZIS indicates that Ru SAs are anchored on ZIS via Ru−S coordination, which is further validated by the appearance of Ru−S coordination in the corresponding wavelet transform contour plots (Figure 2d−f). On the basis of the aforementioned results, Ru atoms in Ru-ZIS present as isolated state on ZIS in the form of Ru−S coordination. Given the higher electronegativity of S than Ru, the electrons will transfer from Ru to S as a result of strong interaction between Ru and S species in Ru-ZIS.

Considering the electron-rich S sites can reduce the binding energy toward *H,[30,31] Ru-ZIS was used as a catalyst for photocatalytic pure water splitting in the absence of sacrificial reagents. First, screening experiments display that the optimal loading amount of Ru on ZIS is 1.3 wt %, namely, Ru-ZIS in following tests (Figures S7−S9 and Table S2). For photocatalytic water splitting, ZIS exhibited poor photocatalytic activity under visible light irradiation ($\lambda \geq 420$ nm) (Figure 3a). In sharp contrast, the evolution rate of H_2 increased to 735.2 μmol g^{-1} h^{-1} when Ru-ZIS was used as the catalyst, thereby suggesting that the introduction of Ru SAs onto ZIS could significantly facilitate photocatalytic water splitting (Figure 3a). When the simulated solar light source (i.e., AM 1.5G, $\lambda \geq 300$ nm) was used, the H_2 productivities of Ru-ZIS and ZIS increased to 1515.8 and 50.6 μmol g^{-1} h^{-1}, respectively (Figure 3b,c), which suggests that the introduction of Ru SAs can largely promote the photocatalytic performance, while only ultraviolet light can trigger H_2 evolution on pure ZIS. Moreover, we synthesized Ru nanoparticles on ZIS nanosheets (Ru_{NPs}-ZIS) as the reference for photocatalytic water splitting (see detailed information in the Supporting Information Experimental Section, Figure S10). The much higher H_2 productivity of Ru-ZIS compared with Ru_{NPs}-ZIS demonstrates that the incorporation of Ru SAs can largely promote H_2 evolution from pure water splitting. To evaluate the performance toward photocatalytic water splitting, the apparent quantum efficiency (AQE) of Ru-ZIS for H_2 evolution was calculated under the irradiation of monochromatic light. The AQE of Ru-ZIS has a maximum value of 7.5% at 420 nm (Figure 3d), and the quantum yield of H_2 evolution decreases with increasing wavelength. This indicates that visible light really drives the H_2 evolution reaction and that the reaction rate is governed by the light absorption properties of Ru-ZIS. The wavelength-dependent performance suggests that Ru-ZIS can absorb light with a broad wavelength range to trigger photocatalytic water splitting to form H_2 (Figures S11 and S12 and Tables S3 and S4). When the light was switched off, no H_2 was produced on Ru-ZIS, thereby demonstrating that water splitting was, indeed, triggered by light irradiation (Figure 3e). Impressively, the solar-to-hydrogen (STH) efficiency reaches ∼0.58%, significantly higher than the value for natural synthetic plants (∼0.10%). Impressively, the stability of Ru-ZIS was highlighted by the steady H_2 productivity after exposing it to ambient environment for 330 days (Figure 3f). In addition, the promising stability of Ru-ZIS was proved by the gradually increasing H_2 productivity within 15 h (Figure S13) and the reserved morphology (Figure S14) and structure (Figure S15) after the durability test. Note that the performance of Ru-ZIS toward photocatalytic pure water splitting has already outperformed many reported catalysts (Figure 3g and Table S5).

To reveal the mechanism for the enhanced performance toward water splitting, ultraviolet−visible (UV−vis) absorption spectroscopy was conducted to evaluate the photoabsorbance of Ru-ZIS and ZIS. After introducing Ru SAs, the color changes from bright yellow to brown, as a result of enhanced light absorption in the range of 200−800 nm (Figure 4a,b).[32] Moreover, the band positions were determined by combining the valence band (VB) energy (Figures S16 and S17) and conduction band (CB) on the basis of the Mott−Schottky plots (Figure S18). The conduction bands (CB) of Ru-ZIS and ZIS were calculated to be −0.77 and −0.44 V (vs RHE), respectively (Figure S18), which suggests that pure water splitting to H_2 is feasible on both ZIS and Ru-ZIS (Figure S19). Furthermore, the steady-state photoluminescence (PL) spectra were collected to investigate the possible recombination of photogenerated carriers. The PL intensity of Ru-ZIS is much lower than that of ZIS, which suggests that the recombination of photogenerated carriers is strongly suppressed after the introduction of Ru SAs (Figure S20).[33,34] Besides, the average lifetime of photogenerated carriers for Ru-ZIS is 3.72 ns, much longer than that of pristine ZIS (0.68 ns), thereby implying that the introduction of Ru SAs can promote the separation of photogenerated electrons and holes (Figure S21 and Table S6).[35,36] Moreover, higher photocurrent intensity means more charge carriers would be generated rapidly, thereby allowing for their separation/transmission as assessed by transient photocurrent response, as shown in Figure S22a.[37] Besides, the diameter of the Nyquist circle of Ru-ZIS (Figure S22b) is much smaller than that of pure ZIS. This proved that the Ru-ZIS has ultrahigh electron conductivity and the lowest charge transfer resistance (Table S7).[38] The reaction barriers of H_2 evolution could be evaluated by linear sweep voltammetry (LSV).[39] As shown in Figure S22c, the LSV curves of Ru-ZIS present smaller onset potentials yet larger current densities than those over ZIS. This implies that the reaction barrier for H_2 evolution could be significantly reduced by the introduction of Ru, thereby indicating more active sites can be induced by Ru doping. Analysis on the steady-state surface photovoltage spectroscopy (SPV), with much stronger SPV signal of Ru-ZIS than that of ZIS (Figure 4c), confirms that the introduction of Ru SAs can facilitate the separation of photogenerated electrons and holes.[40]

In the *in situ* EPR spectra of Ru-ZIS collected under light irradiation, the characteristic signals of Ru^{3+} gradually decrease with the increased irradiation time, which is ascribed to the oxidation of Ru^{3+} (Figure 4d), which suggests that the photogenerated electrons may transfer from Ru to ZIS. Moreover, the transfer from Ru SAs to ZIS in Ru-ZIS was further investigated by analyzing XANES and XPS spectra. The positive shift of K-edge in the XANES spectrum of Ru-ZIS (Figure 4e) and negative shifts of peak in the Zn 2p, In 3d, and S 2p XPS spectra of Ru-ZIS after light irradiation (Figure 4f and Figure S23) indicate that the photogenerated electrons will transfer from Ru SAs to ZIS. Given the strong electron affinity of S, the photoelectrons are finally accumulated on S sites, which leads to the formation of the electron-rich $S^{\delta-}$ as a result of enhanced separation of electron−hole pairs and H_2

https://doi.org/10.1021/prechem.4c00035
Precis. Chem. 2024, 2, 471−479

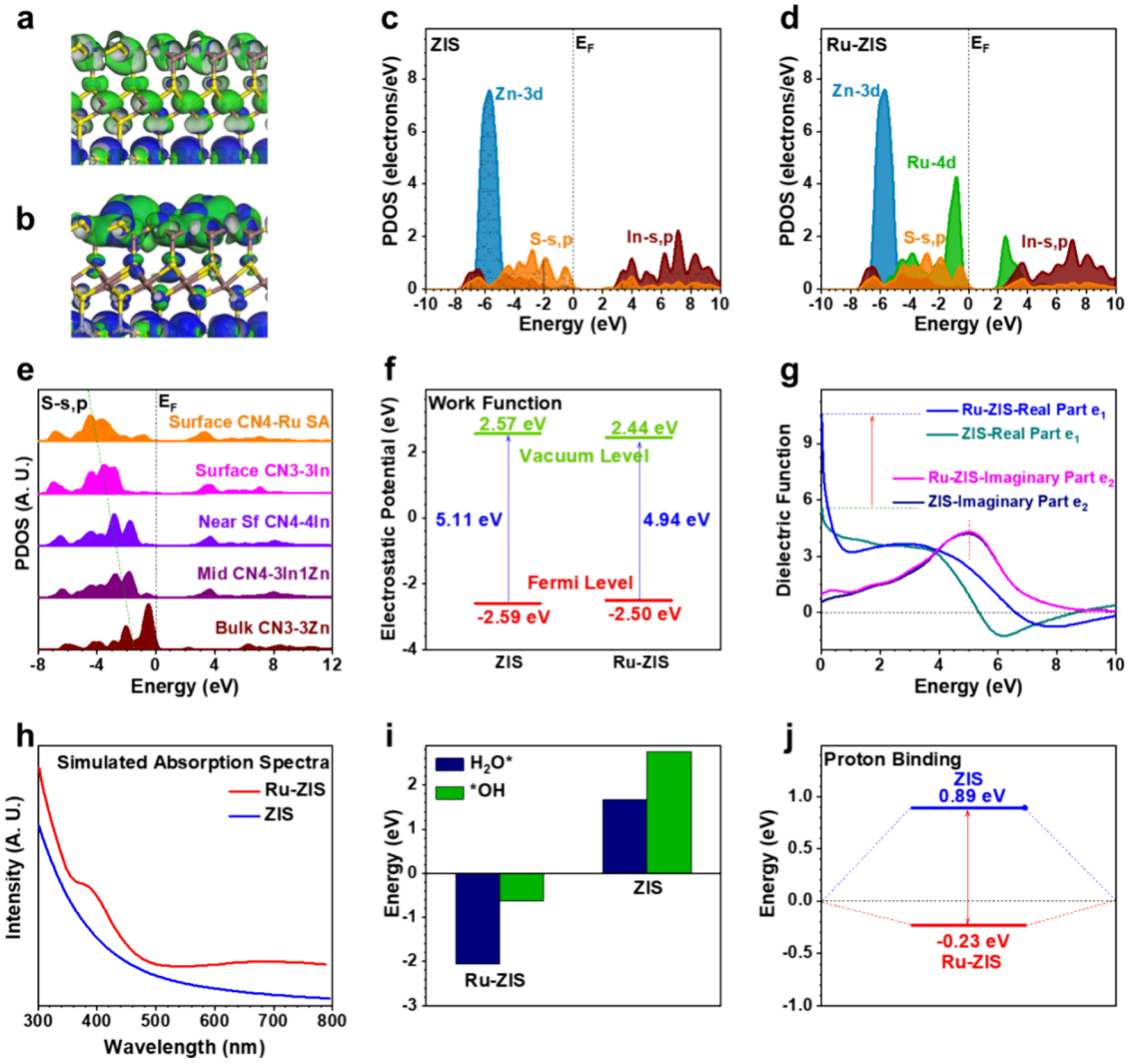

Figure 5. Density functional theory calculations. 3D contour plot of electronic distributions near the Fermi level of (a) ZIS and (b) Ru-ZIS. Green balls, Ru; blue balls, Zn; brown balls, In; yellow balls, S. Blue isosurface, bonding orbitals; green isosurface, antibonding orbitals. PDOS of (c) ZIS and (d) Ru-ZIS. Site-dependent PDOS of (e) S s,p in Ru-ZIS. The (f) work function, (g) dielectric function, and (h) optical absorption comparisons of ZIS and Ru-ZIS. (i) Average adsorption energy comparisons of *H_2O and *OH on ZIS and Ru-ZIS. (j) The proton binding energy of ZIS and Ru-ZIS.

evolution rate (Figure 4g). In contrast, the peak positions in the Zn 2p, In 3d, and S 2p XPS spectra of ZIS remain unchanged after light irradiation (Figure S24), thereby further confirming that the strong synergy between Ru SAs and ZIS can greatly promote the separation of photogenerated electron−hole pairs.

To further demonstrate the significance of the Ru−S channel on the separation of electron−hole pairs and the enhancement of the H_2 evolution rate, Ru-ZIS was treated in H_2 (Ru-ZIS/H_2) and then used as the photocatalyst for water splitting. Note that H_2 treatment leads to the reduction of Ru species in Ru-ZIS, as evidenced by the negative shifts of the peak in the Ru 3d XPS spectrum and the Ru K-edge XANES spectrum of Ru-ZIS/H_2 (Figure S25a,b). Meanwhile, the absence of Ru^{3+} peaks in the EPR spectrum of Ru-ZIS/H_2 further confirms that the Ru−S channel has been partially destroyed (Figure S25d). Compared with Ru-ZIS, the H_2 productivity of Ru-ZIS/H_2 sharply decreases (Figure S26), which further confirms the significance of the Ru−S channel on photocatalytic water splitting. Given that H_2 is the only product from water splitting without any sacrificial agent (Figure S27), the photogenerated holes may be consumed by the photocatalyst. To reveal the reaction pathways, *in situ* EPR measurement was conducted to capture the potential radicals during photocatalytic water splitting. With light irradiation, four characteristic signals of •OH with an intensity ratio of 1:2:2:1 appear in the EPR spectrum of Ru-ZIS (Figure S28a). Besides, the formation of •OH induced by light irradiation was further validated by PL spectroscopy using terephthalic acid (TA) as the probe molecule (Figure S28b).[41] Given the absence of O_2 and H_2O_2 in the products, •OH may further oxidize Ru-ZIS. We compared the Ru 3d, Zn 2p, In 3d, and S 2p of the fresh and spent Ru-ZIS to track the holes. The presence of a peak of Zn−O in the Zn 2p XPS spectrum of Ru-ZIS suggests that partial Zn−S has been oxidized to Zn−O (Figure S29). However, no obvious changes were observed in the S 2p XPS spectrum after light irradiation, which suggests that S species may be oxidized to gaseous sulfur compound (e.g., SO_2) and subsequently desorbs from the spent Ru-ZIS. On the basis of the above results, the reaction pathways for

https://doi.org/10.1021/prechem.4c00035
Precis. Chem. 2024, 2, 471−479

photocatalytic water splitting without sacrificial agent were summarized as follows:

$$\text{Ru-ZIS} + h\nu \rightarrow h^+ + e^- \quad (1)$$

$$3H_2O + 3h^+ \rightarrow 3H^+ + 3OH\bullet \quad (2)$$

$$3OH\bullet + 3h^+ \rightarrow 3O\bullet + 3H^+ \quad (3)$$

$$6H^+ + 6e^- \rightarrow 3H_2 \quad (4)$$

$$3O\bullet + Zn - S \rightarrow Zn - O + SO_2 \quad (5)$$

DFT calculations were employed to investigate the electronic structures and reaction energy changes to reveal the superior photocatalytic performance of Ru-ZIS to that of ZIS for photocatalytic pure water splitting. For the electronic distributions near the Fermi level (E_F), the surface of ZIS was dominated by the antibonding orbitals as a result of low electron transfer efficiency and binding preferences for the H_2O molecules (Figure 5a). After Ru SAs were introduced on the surface, the overall lattice structure was slightly distorted, thereby indicating the stability of the photocatalyst (Figure 5b). More importantly, surface Ru atoms dominated the bonding orbitals with strong coupling with antibonding orbitals, which suggested that the Ru single atoms played an important role in modulating the electronic structure. The projected partial density of states (PDOSs) would further unravel the detailed contributions of different elements (Figure 5c). For the ZIS structure, the Zn 3d orbitals delivered a sharp peak at a deep position of E_V = 5.7 eV, which led to limited contributions to the band structure. Notably, the valence band maximum (VBM) was mainly dominated by S s,p orbitals, while the conduction band minimum (CBM) was constructed by both S s,p and In s,p orbitals. A new band gap of 2.37 eV was observed between the CBM and VBM, which was in line with experimental results. As shown in Figure 5d, Ru SAs strongly contributed to both CBM and VBM, which resulted in band gap alleviations from 2.37 to 2.02 eV as a result of enhanced charge separation and transfer process to promote photocatalysis. The PDOS of Zn 3d and In s,p in Ru-ZIS remained similar to that of ZIS, which was consistent with the stable structure even after the introduction of Ru SAs.

Moreover, the site-dependent PDOS of S s,p orbitals further uncovered the interactions between S and Ru atoms (Figure 5e). For S sites coordinated with 3 Zn atoms at the bottom of the ZIS layered structure, the s,p orbitals located close to the E_F continuously downshifted from midlattice to the surface with different coordination environments. Moreover, the surface S atoms that anchoring Ru SAs exhibited a further downshifting of the s,p orbitals, which was attributed to the electron transfer from Ru to the S sites, being consistent with XPS results. In addition, the introduction of Ru SAs led to the work function change of the photocatalyst surface (Figure 5f). Compared with ZIS, the Fermi level in Ru-ZIS slightly increased, while the overall work function decreased from 5.11 to 4.94 eV, which favored the electron depletion to the photocatalyst surface and the adsorbates. Meanwhile, the optical properties were further studied by dielectric function analysis and simulated absorption spectra (Figure 5g). For the dielectric function, the intercept of real part ε_1 indicates the value of dielectric constants, while the first peak of the imaginary part ε_2 represents the bonding environments in the lattice. The introduction of Ru SAs resulted in evident increases in the dielectric constant, which promoted charge separation and transfer due to a decrease of the exciton binding energy. Accordingly, the lifetime of the charge carriers was prolonged, which agreed with the time-resolved transient PL decay spectra. Note that negligible influence on ε_2 peak after introducing Ru SAs indicated the stable structure of Ru-ZIS. Moreover, Ru-ZIS also shows an overall improved absorption intensity in the visible light range (300−800 nm). As shown in Figure 5h, an intense peak at ∼385 nm in the simulated absorption spectrum of Ru-ZIS, which was close to the experimental absorption spectrum, further supports improved H_2 productivity under irradiation with 400 nm light. These results indicated that Ru SAs in ZIS significantly improved the electronic structures and optical properties, which contributed to the enhanced photocatalytic properties.

Additionally, DFT calculations were conducted to evaluate the adsorption of key intermediates on Ru-ZIS and ZIS (Figure 5i). Compared with ZIS, Ru-ZIS displayed a much stronger adsorption ability toward H_2O, which promoted the generation of H^+ and •OH. Furthermore, Ru-ZIS displayed a mild binding to proton with an adsorption energy of −0.23 eV, which was much lower than that of ZIS (0.89 eV), thereby suggesting that Ru-ZIS favored H_2 generation (Figure 5j). Consequently, DFT calculations suggested that doping ZIS with Ru SAs could construct charge transfer channels as a result of enhanced separation of photogenerated electron−hole pairs. With the enhanced electronic structures and optical properties, the energy barrier for water dissociation on Ru-ZIS was much lower than that of ZIS, which led to the significant enhancement on photocatalytic activity.

3. CONCLUSION

In this work, we successfully constructed charge transfer channels in ZIS after doping Ru SAs. Under light irradiation, the photogenerated electrons can transfer from Ru SAs to S sites through the Ru−S channel, which leads to the enhanced separation of electron−hole pairs. Consequently, Ru-ZIS can serve as an efficient catalyst for photocatalytic pure water splitting without sacrificial agent to produce H_2. The productivity of H_2 for Ru-ZIS reaches 735.2 μmol g^{-1} h^{-1} under visible light irradiation in the absence of any sacrificial agents, which is ∼30 times higher than that of ZIS, and has surpassed many reported photocatalysts for water splitting. Impressively, the AQE of Ru-ZIS for H_2 evolution reaches 7.5% at 420 nm with an STH efficiency of 0.58%, which is much higher than the value of natural synthetic plants (∼0.10%). This work provides a highly efficient strategy for the separation of photogenerated electron−hole pairs, which may motivate fundamental research for photocatalytic water splitting.

■ ASSOCIATED CONTENT

Supporting Information

The Supporting Information is available free of charge at https://pubs.acs.org/doi/10.1021/prechem.4c00035.

Materials, synthesis, physical characterizations, and other spectral characterization of Ru-ZIS, as well as Figures S1−S29 and Tables S1−S7 (PDF)

https://doi.org/10.1021/prechem.4c00035
Precis. Chem. 2024, 2, 471−479

AUTHOR INFORMATION

Corresponding Authors

Bolong Huang − *Department of Applied Biology and Chemical Technology, The Hong Kong Polytechnic University, Kowloon, Hong Kong SAR 999077, China;* orcid.org/0000-0002-2526-2002; Email: bhuang@polyu.edu.hk

Yong Xu − *i-lab, Suzhou Institute of Nano-Tech and Nano-Bionics (SINANO), Chinese Academy of Sciences (CAS), Suzhou 215123, China;* orcid.org/0000-0001-5115-6492; Email: yxu2023@sinano.ac.cn

Xiaoqing Huang − *State Key Laboratory of Physical Chemistry of Solid Surfaces, College of Chemistry and Chemical Engineering, Xiamen University, Xiamen 361005, China;* orcid.org/0000-0003-3219-4316; Email: hxq006@xmu.edu.cn

Authors

Huiping Peng − *State Key Laboratory of Physical Chemistry of Solid Surfaces, College of Chemistry and Chemical Engineering, Xiamen University, Xiamen 361005, China*

Mingzi Sun − *Department of Applied Biology and Chemical Technology, The Hong Kong Polytechnic University, Kowloon, Hong Kong SAR 999077, China;* orcid.org/0000-0001-5136-7265

Fei Xue − *State Key Laboratory of Physical Chemistry of Solid Surfaces, College of Chemistry and Chemical Engineering, Xiamen University, Xiamen 361005, China*

Xiaozhi Liu − *Beijing National Laboratory for Condensed Matter Physics Institute of Physics, Chinese Academy of Sciences, Beijing 100190, China;* orcid.org/0000-0001-8647-8694

Shangheng Liu − *State Key Laboratory of Physical Chemistry of Solid Surfaces, College of Chemistry and Chemical Engineering, Xiamen University, Xiamen 361005, China*

Tang Yang − *State Key Laboratory of Physical Chemistry of Solid Surfaces, College of Chemistry and Chemical Engineering, Xiamen University, Xiamen 361005, China*

Lin Sun − *State Key Laboratory of Physical Chemistry of Solid Surfaces, College of Chemistry and Chemical Engineering, Xiamen University, Xiamen 361005, China*

Hongbo Geng − *School of Materials Engineering, Changshu Institute of Technology, Changshu 215500, China*

Dong Su − *Beijing National Laboratory for Condensed Matter Physics Institute of Physics, Chinese Academy of Sciences, Beijing 100190, China;* orcid.org/0000-0002-1921-6683

Complete contact information is available at: https://pubs.acs.org/10.1021/prechem.4c00035

Author Contributions

X.H. and Y.X. conceived and supervised the research. X.H., Y.X., and H.P. analyzed the data. H.P., M.S., F.X., S.L., T.Y., L.S., and H.G. performed the experiments and characterizations. X.L. and D.S. performed partial TEM measurements. M.S. and B.H. conducted DFT calculations. X.H., Y.X., and H.P. wrote the manuscript.

Notes

The authors declare no competing financial interest.

ACKNOWLEDGMENTS

This work was financially supported by the National Key R&D Program of China (2020YFB1505802), the Ministry of Science and Technology (2017YFA0208200), the National Natural Science Foundation of China (22025108, U21A20327, and 22121001), and the start-up funding from Xiamen University. The authors thank beamline BL14W1 (Shanghai Synchrotron Radiation Facility) for providing the beam time.

REFERENCES

(1) Wang, P.; Luo, Y.; Zhang, G.; Wu, M.; Chen, Z.; Sun, S.; Shi, Z. MnO_x-decorated nickel-iron phosphides nanosheets: interface modifications for robust overall water splitting at ultra-high current densities. *Small* **2022**, *18* (7), 2105803.

(2) Zhu, S.; Qin, X.; Xiao, F.; Yang, S.; Xu, Y.; Tan, Z.; Li, J.; Yan, J.; Chen, Q.; Chen, M.; Shao, M. The role of ruthenium in improving the kinetics of hydrogen oxidation and evolution reactions of platinum. *Nat. Catal.* **2021**, *4*, 711−718.

(3) Feng, R.; Wan, K.; Sui, X.; Zhao, N.; Li, H.; Lei, W.; Yu, J.; Liu, X.; Shi, X.; Zhai, M.; Liu, G.; Wang, H.; Zheng, L.; Liu, M. Anchoring single Pt atoms and black phosphorene dual co-catalysts on CdS nanospheres to boost visible-light photocatalytic H_2 evolution. *Nano Today* **2021**, *37*, 101080.

(4) Sun, S.; Shen, G.; Jiang, J.; Mi, W.; Liu, X.; Pan, L.; Zhang, X.; Zou, J.-J. Boosting oxygen evolution kinetics by Mn-N-C motifs with tunable spin state for highly efficient solar-driven water splitting. *Adv. Energy Mater.* **2019**, *9* (30), 1901505.

(5) Chen, R.; Zhuang, G.-L.; Wang, Z.-Y.; Gao, Y.-J.; Li, Z.; Wang, C.; Zhou, Y.; Du, M.-H.; Zeng, S.; Long, L.-S.; Kong, X.-J.; Zheng, L.-S. Integration of bio-inspired lanthanide-transition metal cluster and P-doped carbon nitride for efficient photocatalytic overall water splitting. *Natl. Sci. Rev.* **2021**, *8* (9), nwaa234.

(6) Han, Q.; Wu, C.; Jiao, H.; Xu, R.; Wang, Y.; Xie, J.; Guo, Q.; Tang, J. Rational design of high-concentration Ti^{3+} in porous carbon-doped TiO_2 nanosheets for efficient photocatalytic ammonia synthesis. *Adv. Mater.* **2021**, *33* (9), 2008180.

(7) Sekar, K.; Chuaicham, C.; Vellaichamy, B.; Li, W.; Zhuang, W.; Lu, X.; Ohtani, B.; Sasaki, K. Cubic Cu_2O nanoparticles decorated on TiO_2 nanofiber heterostructure as an excellent synergistic photocatalyst for H_2 production and sulfamethoxazole degradation. *Appl. Catal. B: Environ.* **2021**, *294*, 120221.

(8) Wei, Z.; Wang, W.; Li, W.; Bai, X.; Zhao, J.; Tse, E. C. M.; Phillips, D. L.; Zhu, Y. Steering electron-hole migration pathways using oxygen vacancies in tungsten oxides to enhance their photocatalytic oxygen evolution performance. *Angew. Chem., Int. Ed.* **2021**, *60* (15), 8236−8242.

(9) Bie, C.; Zhu, B.; Xu, F.; Zhang, L.; Yu, J. In situ grown monolayer N-doped graphene on CdS hollow spheres with seamless contact for photocatalytic CO_2 reduction. *Adv. Mater.* **2019**, *31*, 1902868.

(10) Li, P.; Chen, X.; He, H.; Zhou, X.; Zhou, Y.; Zou, Z. Polyhedral faceted $BiVO_4$ microcrystals predominantly enclosed by high-index planes promoting photocatalytic water-splitting activity. *Adv. Mater.* **2018**, *30*, 1703119.

(11) Wang, C.; Wang, K.; Feng, Y.; Li, C.; Zhou, X.; Gan, L.; Feng, Y.; Zhou, H.; Zhang, B.; Qu, X.; Li, H.; Li, J.; Li, A.; Sun, Y.; Zhang, S.; Yang, G.; Guo, Y.; Yang, S.; Zhou, T.; Dong, F.; Zheng, K.; Wang, L.; Huang, J.; Zhang, Z.; Han, X. Co and Pt dual-single-atoms with oxygen-coordinated Co-O-Pt dimer sites for ultrahigh photocatalytic hydrogen evolution efficiency. *Adv. Mater.* **2021**, *33* (13), 2003327.

(12) Liu, Y.; Liu, C.-H.; Debnath, T.; Wang, Y.; Pohl, D.; Besteiro, L. V.; Meira, D. M.; Huang, S.; Yang, F.; Rellinghaus, B.; Chaker, M.; Perepichka, D. F.; Ma, D. Silver nanoparticle enhanced metal-organic matrix with interface-engineering for efficient photocatalytic hydrogen evolution. *Nat. Commun.* **2023**, *14*, 541.

(13) Zhang, C.; Xie, C.; Gao, Y.; Tao, X.; Ding, C.; Fan, F.; Jiang, H.-L. Charge separation by creating band bending in metal-organic

frameworks for improved photocatalytic hydrogen evolution. *Angew. Chem., Int. Ed.* **2022**, *61*, No. e202204108.
(14) Sheng, H.; Wang, J.; Huang, J.; Li, Z.; Ren, G.; Zhang, L.; Yu, L.; Zhao, M.; Li, X.; Li, G.; Wang, N.; Shen, C.; Lu, G. Strong synergy between gold nanoparticles and cobalt porphyrin induces highly efficient photocatalytic hydrogen evolution. *Nat. Commun.* **2023**, *14*, 1528.
(15) Wang, S.; Wang, Y.; Zhang, S. L.; Zang, S.-Q.; Lou, X. W. D. Supporting ultrathin $ZnIn_2S_4$ nanosheets on Co/N-doped graphitic carbon nanocages for efficient photocatalytic H_2 generation. *Adv. Mater.* **2019**, *31*, 1903404.
(16) Si, S.; Shou, H.; Mao, Y.; Bao, X.; Zhai, G.; Song, K.; Wang, Z.; Wang, P.; Liu, Y.; Zheng, Z.; Dai, Y.; Song, L.; Huang, B.; Cheng, H. Low-coordination single Au atoms on ultrathin $ZnIn_2S_4$ nanosheets for selective photocatalytic CO_2 reduction towards CH_4. *Angew. Chem., Int. Ed.* **2022**, *61* (41), No. e202209446.
(17) Shi, X.; Mao, L.; Yang, P.; Zheng, H.; Fujitsuka, M.; Zhang, J.; Majima, T. Ultrathin $ZnIn_2S_4$ nanosheets with active (110) facet exposure and efficient charge separation for cocatalyst free photocatalytic hydrogen evolution. *Appl. Catal. B: Environ.* **2020**, *265*, 118616.
(18) Li, J.; Tan, C.; Qi, M.; Tang, Z.; Xu, Y. Exposed zinc sites on hybrid $ZnIn_2S_4$@CdS nanocages for efficient regioselective photocatalytic epoxide alcoholysis. *Angew. Chem., Int. Ed.* **2023**, *62*, No. e202303054.
(19) Zhao, D.; Wang, Y.; Dong, C.-L.; Huang, Y.-C.; Chen, J.; Xue, F.; Shen, S.; Guo, L. Boron-doped nitrogen-deficient carbon nitride-based Z-scheme heterostructures for photocatalytic overall water splitting. *Nat. Energy* **2021**, *6*, 388−397.
(20) Wu, X.; Zhang, H.; Zuo, S.; Dong, J.; Li, Y.; Zhang, J.; Han, Y. Engineering the coordination sphere of isolated active sites to explore the intrinsic activity in single-atom catalysts. *Nano-Micro Lett.* **2021**, *13*, 136.
(21) Zhang, X.; Huang, W.; Yu, L.; García Melchor, M.; Wang, D.; Zhi, L.; Zhang, H. Enabling heterogeneous catalysis to achieve carbon neutrality: Directional catalytic conversion of CO_2 into carboxylic acids. *Carbon Energy* **2024**, *6* (3), No. e362.
(22) Kong, M.; Li, Y.; Chen, X.; Tian, T.; Fang, P.; Zheng, F.; Zhao, X. Tuning the relative concentration ratio of bulk defects to surface defects in TiO_2 nanocrystals leads to high photocatalytic efficiency. *J. Am. Chem. Soc.* **2011**, *133*, 16414−16417.
(23) Pastor, E.; Sachs, M.; Selim, S.; Durrant, J.; Bakulin, A.; Walsh, A. Electronic defects in metal oxide photocatalysts. *Nat. Rev. Mater.* **2022**, *7*, 503−521.
(24) Jiang, Y.; Li, S.; Wang, S.; Zhang, Y.; Long, C.; Xie, J.; Fan, X.; Zhao, W.; Xu, P.; Fan, Y.; Cui, C.; Tang, Z. Enabling specific photocatalytic methane oxidation by controlling free radical type. *J. Am. Chem. Soc.* **2023**, *145* (4), 2698−2707.
(25) Sun, Y.; Ding, S.; Xia, B.; Duan, J.; Antonietti, M.; Chen, S. Biomimetic FeMo(Se, Te) as joint electron pool promoting nitrogen electrofixation. *Angew. Chem., Int. Ed.* **2022**, *61*, No. e202115198.
(26) Zhang, Y.; Ding, Z.; Foster, C. W.; Banks, C. E.; Qiu, X.; Ji, X. Oxygen vacancies evoked blue TiO_2(B) nanobelts with efficiency enhancement in sodium storage behaviors. *Adv. Funct. Mater.* **2017**, *27*, 1700856.
(27) Blazey, K.W.; Muller, K.A.; Berlinger, W.; Triggs, P.; Levy, F. Paramagnetic Ru^{5+} and Ru^{3+} centers in TiO_2: Ru. *Solid State Commun.* **1985**, *54*, 1039−1041.
(28) Zhang, H.; Zuo, S.; Qiu, M.; Wang, S.; Zhang, Y.; Zhang, J.; Lou, X. W. D. Direct probing of atomically dispersed Ru species over multi-edged TiO_2 for highly efficient photocatalytic hydrogen evolution. *Sci. Adv.* **2020**, *6* (39), 9823.
(29) Luo, N.; Montini, T.; Zhang, J.; Fornasiero, P.; Fonda, E.; Hou, T.; Nie, W.; Lu, J.; Liu, J.; Heggen, M.; Lin, L.; Ma, C.; Wang, M.; Fan, F.; Jin, S.; Wang, F. Visible-light-driven coproduction of diesel precursors and hydrogen from lignocellulose-derived methylfurans. *Nat. Energy* **2019**, *4*, 575−584.
(30) Shi, X.; Dai, C.; Wang, X.; Hu, J.; Zhang, J.; Zheng, L.; Mao, L.; Zheng, H.; Zhu, M. Protruding Pt single-sites on hexagonal $ZnIn_2S_4$ to accelerate photocatalytic hydrogen evolution. *Nat. Commun.* **2022**, *13*, 1287.
(31) Gao, D.; Xu, J.; Wang, L.; Zhu, B.; Yu, H.; Yu, J. Optimizing atomic hydrogen desorption of sulfur-rich NiS_{1+x} cocatalyst for boosting photocatalytic H_2 evolution. *Adv. Mater.* **2022**, *34*, 2108475.
(32) Zhu, Y.; Lv, C.; Yin, Z.; Ren, J.; Yang, X.; Dong, C.; Liu, H.; Cai, R.; Huang, Y.; Theis, W.; Shen, S.; Yang, D. A [001]-oriented hittorf's phosphorus nanorods/polymeric carbon nitride heterostructure for boosting wide-spectrum-responsive photocatalytic hydrogen evolution from pure water. *Angew. Chem., Int. Ed.* **2020**, *59*, 868.
(33) Huang, W.; Bo, T.; Zuo, S.; Wang, Y.; Chen, J.; Ould Chikh, S.; Li, Y.; Zhou, W.; Zhang, J.; Zhang, H. Surface decorated Ni sites for superior photocatalytic hydrogen production. *Susmat* **2022**, *2*, 466−475.
(34) Wang, W.-K.; Chen, J.-J.; Lou, Z.-Z.; Kim, S.; Fujitsuka, M.; Yu, H.-Q.; Majima, T. Single-molecule and particle probing crystal edge/corner as highly efficient photocatalytic sites on a single TiO_2 particle. *Proc. Natl. Acad. Sci. U.S.A.* **2019**, *116*, 18827−18833.
(35) Hao, M.; Bai, Y.; Zeiske, S.; Ren, L.; Liu, J.; Yuan, Y.; Zarrabi, N.; Cheng, N.; Ghasemi, M.; Chen, P.; Lyu, M.; He, D.; Yun, J.-H.; Du, Y.; Wang, Y.; Ding, S.; Armin, A.; Meredith, P.; Liu, G.; Cheng, H.-M.; Wang, L. Ligand-assisted cation-exchange engineering for high-efficiency colloidal $Cs_{1-x}FA_xPbI_3$ quantum dot solar cells with reduced phase segregation. *Nat. Energy* **2020**, *5*, 79−88.
(36) Feng, C.; Bo, T.; Maity, P.; Zuo, S.; Zhou, W.; Huang, K. W.; Mohammed, O. F.; Zhang, H. B. Regulating photocatalytic CO_2 reduction kinetics through modification of surface coordination sphere. *Adv. Funct. Mater.* **2023**, *34* (9), 2309761.
(37) Dai, B.; Fang, J.; Yu, Y.; Sun, M.; Huang, H.; Lu, C.; Kou, J.; Zhao, Y.; Xu, Z. Construction of infrared-light-responsive photo-induced carriers driver for enhanced photocatalytic hydrogen evolution. *Adv. Mater.* **2020**, *32*, 1906361.
(38) Ruan, X.; Huang, C.; Cheng, H.; Zhang, Z.; Cui, Y.; Li, Z.; Xie, T.; Ba, K.; Zhang, H.; Zhang, L.; Zhao, X.; Leng, J.; Jin, S.; Zhang, W.; Zheng, W.; Ravi, S. K.; Jiang, Z.; Cui, X.; Yu, J. A twin S-scheme artificial photosynthetic system with self-assembled heterojunctions yields superior photocatalytic hydrogen evolution rate. *Adv. Mater.* **2023**, *35*, 2209141.
(39) Su, L.; Wang, P.; Wang, J.; Zhang, D.; Wang, H.; Li, Y.; Zhan, S.; Gong, J. Pt-Cu interaction induced construction of single Pt sites for synchronous electron capture and transfer in photocatalysis. *Adv. Funct. Mater.* **2021**, *31* (47), 2104343.
(40) Xin, Z.; Gao, Y.; Gao, Y.; Song, H.; Zhao, J.; Fan, F.; Xia, A.; Li, X.; Tung, C.; Wu, L. Rational design of dot-on-rod nano-heterostructure for photocatalytic CO_2 reduction: pivotal role of hole transfer and utilization. *Adv. Mater.* **2022**, *34* (3), 2106662.
(41) Moradi, M.; Hasanvandian, F.; Isari, A. A.; Hayati, F.; Kakavandi, B.; Setayesh, S. R. CuO and ZnO co-anchored on g-C_3N_4 nanosheets as an affordable double Z-scheme nanocomposite for photocatalytic decontamination of amoxicillin. *Appl. Catal. B: Environ.* **2021**, *285*, 119838.

https://doi.org/10.1021/prechem.4c00035
Precis. Chem. 2024, 2, 471−479